Electronic Supplementary Material (ESI) for Journal of Materials Chemistry A.
This journal is © The Royal Society of Chemistry 2022

Supplementary Information

Visible and Infrared Solar Upconversion for Water Splitting via Surface Plasmon-passivated Strategy

Ruiting Xue[a,b,*], Chengyuan Huang[a], Jianmin Deng[a], Lei Yang[a], Lei Li[a], Ximei Fan[a,*]

[a]Key Laboratory of Advanced Technologies of Materials, Ministry of Education, School of Materials Science and Engineering, Southwest Jiaotong University, Chengdu 610031, P. R. China

[b]United Technology Center of Western Metal Materials Co.,Ltd, Northwest Institute For Non-ferrous Metal Research, Shaanxi Institute For Materials Engineering, Xi'an 710016, P. R. China

Corresponding author: Ruiting Xue, Ph.D., Email address: xrt55@163.com; Ximei Fan, Ph.D., professor, Email address: xmfan@swjtu.edu.cn

Comparisons of Plasmon-promoted Reaction Mechanisms

It is well known that LSPR improves the catalytic efficiency and it is used for many difficult chemical reactions. However, current understanding of the underlying mechanism is still poorly explored. It is generally accepted that hot electrons excited by LSPR are transferred to the CB or LUMO of the adsorbent by electron-phonon scattering to promote the chemical reaction (Figure S1a). Some latest researches have provided many important advances: the transition of electron vibrational energy level can reduce the reaction barrier (Figure S1b);[1] the lattice expansion caused by electron energy transfer can redshift the absorption band edge (Figure S1c);[2] an additional dephasing channel, namely, chemical interface damping (CID) between the metal and adsorbent can induce the direct transfer of hot electrons (Figure S1d).[3] Figure S1a-c shows the LSPR thermal effect, and this effect is generally of primary interest in current study. This conventional process relies on the thermal vibrations of metal atoms, and the excess energy is transferred to the adsorbent in the form of chemical interface scattering (CIS), where the wave function of the photon collapses and converges to the boundary, that is, the wave form with divergent infinite distribution is transformed into a highly localized particle form. However, to cross the barrier between the metal and adsorbent, plasmonic thermal processes typically require a strong light field; and they are also accompanied by a large amount of energy loss because the thermal transfer is non-directional, which limits their usefulness and energy efficiency. On the contrary, when the CID is present at the interface, the electron wave function of the metal and adsorbent keep continuous in the channel, and photons can maintain wave state and induce electrons to be directly excited to the adsorbent by resonating with plasmonic wave. This direct excitation process requires no additional

activation energy and is therefore not limited by the intensity of the light field. It can be also controlled directionally, thereby has high energy efficiency. This mechanism is the premise of our proposed plasmonic upconversion.

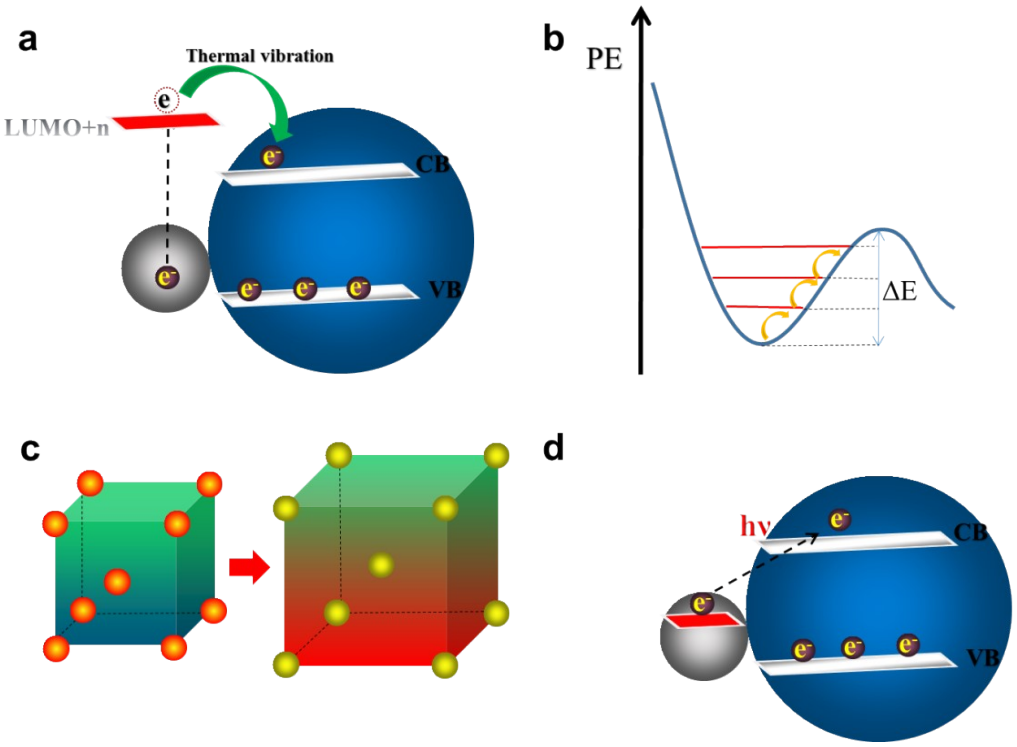

Figure S1: Schematic diagram of LSPR promoting reaction.

Morphology of PDA/ZnO and Elements Mass Ratio of Ag_{-PDA}/ZnO

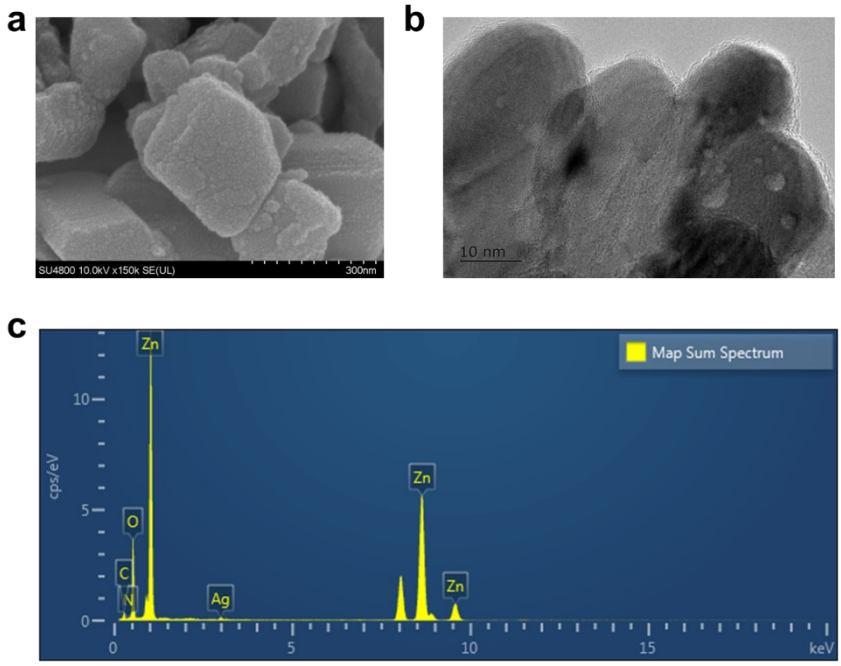

Figure S2: The polymerization morphology of PDA on ZnO surface before Ag in-situ photoreduction. a, SEM image. **b,** TEM image. In the absence of oxygen, the self-polymerization of dopamine was inhibited and the ZnO surface can not be completely coated. Therefore, under UV irradiation, the partially exposed ZnO active site becomes the reduction center of Ag^{+}. After further heat preservation, electron transfer occurs on the composite surface and form a strong interaction interface. **c,** EDS scan results of Ag_{-PDA}/ZnO after Ag in-situ photoreduction.

Table S1 Each element mass ratio of Ag_{-PDA}/ZnO.

Element	Line Type	k factor	Absorption Correction	Wt%	Wt% Sigma
C	K series	2.50675	1.00	2.32	0.19
N	K series	3.14061	1.00	0.47	0.22
O	K series	1.86867	1.00	20.53	0.31
Zn	K series	1.46179	1.00	75.17	0.39

Ag	L series	1.75707	1.00	1.50	0.17
Total:				100.00	

Basic Optical Properties of Ag_{-PDA}/ZnO

The DRS and PL results (Figure S3a,b) evidently presented the best visible light absorption and charge separation efficiency of the Ag_{-PDA}/ZnO with 5% PDA mass ratio. Since the DRS results show such a broad absorption peak, it is important to distinguish the plasmonic response from the interband transition of Ag. In general, plasmonic response wavelength longer than interband transition, and is dominant when the number of free electrons in a metal cluster exceeds 100.[4] In Figure 2a-c, the Ag clusters size exceeds 10 nm, and contains more than 30000 atoms, so the visible light absorption is mainly ascribe to the plasmonic response. Particularly, we further study the size effect of Ag on the light response by controlling the reduction process (Figure S3c). Ag was reduced by irradiation and their sizes, orientation and arrangement are irregular. When a small amount of Ag aggregated (Figure S3d), the interband transition was significant and the plasmonic response was weak. As Ag^+ continued to be reduced and aggregated (Figure S3e), the interband transition was weakened and the plasmonic response was enhanced. When the reduction reaction is complete (Figure S3f), the overall absorption spectrum is further enhanced. The different sizes and orientation would result in different plasmon frequencies, also, absorption peaks are highly determined by the coupling effect of local plasmon which depends on arrangement and surrounding medium.[5] Therefore, when the PDA further tunes the electronic structure of Ag (i.e., diversifies the dielectric environment), the coupling between local plasmon are difficult to produce resonance enhancement, resulting in the feature peaks eliminate completely in 400-800 nm (Figure S3a). Considering the extremely high extinction cross section of Ag and low photon density of solar, we suggest that it is more practical to broaden light absorption range than to enhance a certain LSPR frequency

absorption for solar catalysis via disordered plasmonic electronic structure.

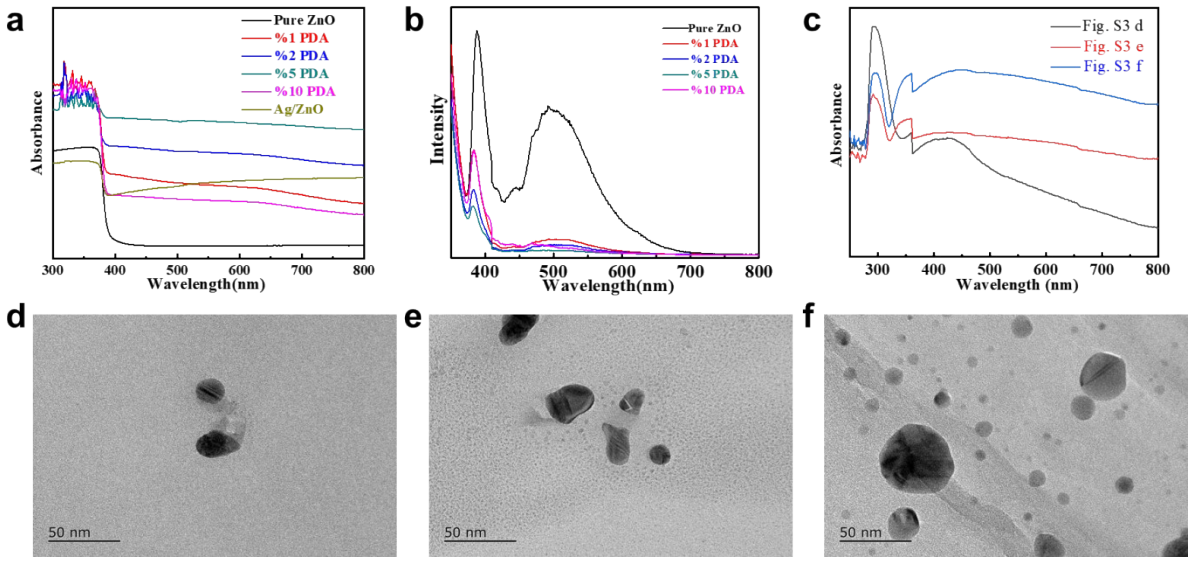

Figure S3: a, UV-Vis DRS spectrum of Ag_{-PDA}/ZnO (PDA mass ratio: 0%, 1%, 2%, 5%, 10%). **b,** PL spectrum of pure ZnO, Ag_{-PDA}/ZnO (PDA mass ratio: 1%, 2%, 5%, 10%), excitation wavelength 325 nm, the strong luminescence peak at about 380 nm is exciton luminescence of ZnO, and the luminescence in the 420~600 nm region is caused by various surface defects in ZnO. **c,** UV-Vis DRS spectrum of Ag clusters (the initial, intermediate and completion of its reduction process). **d-f,** TEM images of Ag clusters (the initial, intermediate and completion of its reduction process).

Upconversion, Time-resolved PL and Transient Absorption

Since Ag_{-PDA}/ZnO produces almost no fluorescence, we verified the upconversion feature by Ag/ZnO with strong metal-support interaction (SMSI). Figure S4a shows that Ag/ZnO produces upconversion fluorescence in the range of 350 to 600 nm under 633 and 908 nm laser excitation. Since two 908 nm photons still do not have enough energy to produce a 380 nm photon, which indicating that the upconversion is induced by LSPR and can involve more than two photons at the same time. The charge transfer mechanism can be further studied by transient absorption (TA) spectroscopy. In Figure S4d, Ag_{-PDA}/ZnO exhibits exciton bleaching (XB) at about 380 nm when excited by 550 nm pump, obviously indicating that LSPR excites electron from Ag to ZnO within 80 fs. Moreover, the excited-LSPR re-absorption is also observed in 550-800 nm region. These features support the claim that LSPR facilitates upconversion at femtosecond scale.[6] When Ag_{-PDA}/ZnO is excited by 350 nm pump (Figure S4c), XB and excited-LSPR re-absorption are rapidly generated within 80 fs and continuously attenuated within a few nanosecond. By contrast, in Figure S4d (550 nm pump), both signals hardly decay within 1 ps and turn to increase in the subsequent time. This charge transfer feature is kinetically consist with the Marcus inverted region.[7] In time-resolved spectrum, instantaneous fluorescence quenching occurs in Ag_{-PDA}/ZnO (Figure S4b, the detected signal is mainly the excitation pulse). According to its sampling principle (inset in Figure S4b), this result represents two possibilities: (i) PDA provides extraordinary fast radiation deactivation channels, so that in the first delay time (t) after excitation, the electrons have been deactivated; (ii) the excited electrons have such a long lifetime that few photon is collected during the detected gate time (Δt). In the EPR results, the number of unpaired electrons keep increasing

with illumination time, indicating that a large number of excited state electrons were not deactivated. Also, in Figure S4d, the enhancement of XB signal on nanosecond scale supports long-lived excited-electrons. Therefore, we are convinced that the excited-electrons transfer to PDA and are eventually deactivated in non-radiative form, which is a extremely long dynamics process (i.e., the second possibility above) and could enter Marcus inverted region.

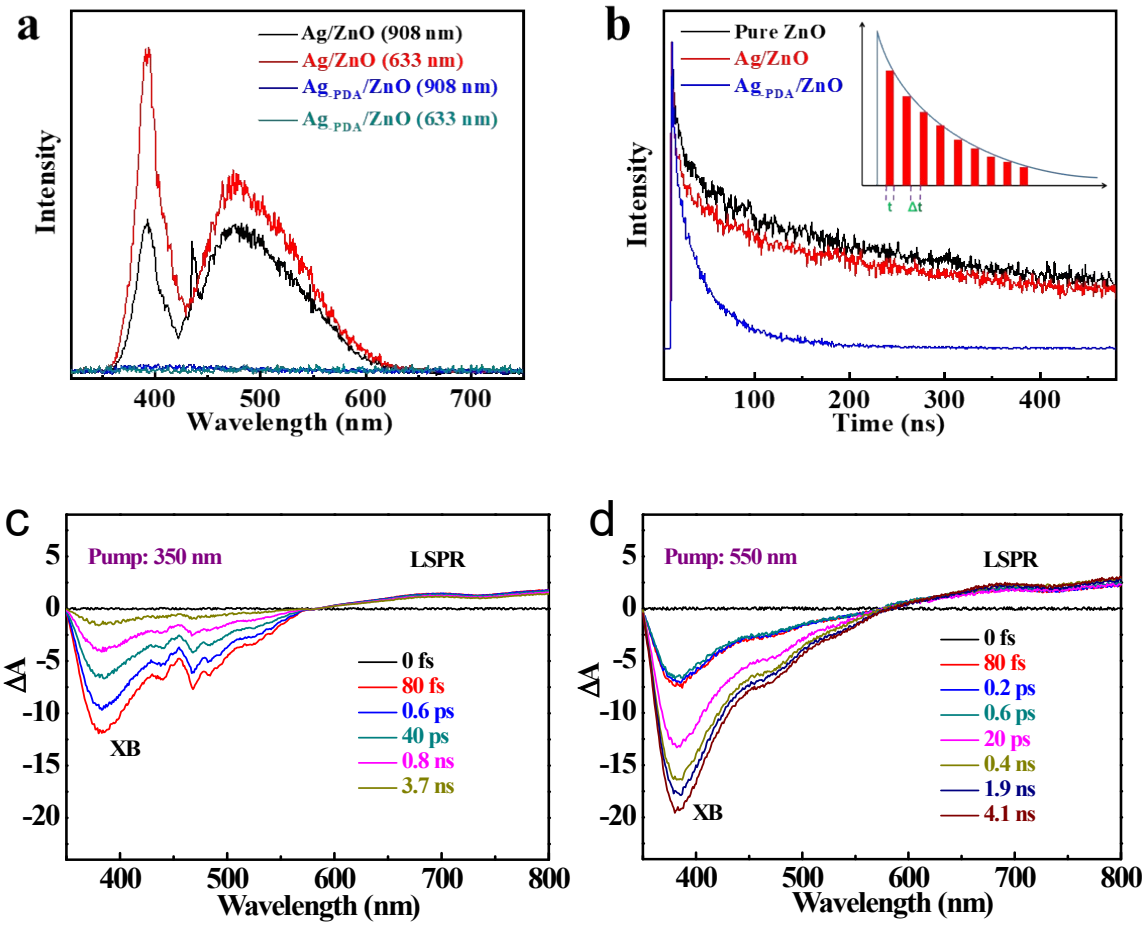

Figure S4: a, PL spectra of Ag/ZnO, Ag_{-PDA}/ZnO, excitation wavelengths are 633 and 908 nm. **b,** Time-resolved spectrum of pure ZnO, Ag/ZnO and Ag_{-PDA}/ZnO. The inset is its grid sampling principle. **c, d,** TA spectra of Ag_{-PDA}/ZnO. (pump wavelength: **c,** 350 nm, **d,** 550 nm; probe wavelength: 350-800 nm). The exciton bleaching of ZnO (about 380 nm) observed at 550 nm pump excitation demonstrates that electron transfer from Ag to ZnO within 80 fs.

Illustration for Direct Electron Excitation Mechanism

The electrons transfer from metal to semiconductor prevents electron-hole recombination, which is the key to plasmonic photocatalyst.[8] Direct excitation is the core mechanism of charge separation in our ternary system,[9] and is analyzed via FDTD simulations (Figure S5a, b). The LSPR-generated electric fields are usually highly localized in quasi-particle form (Figure S5a). Light is absorbed by Ag and localized in the electron wave function on the Ag surface. The electric field generated by contact potential difference mainly occurs on ZnO surface. Therefore, the changing electric field generated by light field is also localized in ZnO lattice to form phonons, which exhibit particle properties. The electron wave function collapses and converges to the boundary, thereby forming its transfer barrier. However, when PDA layer is added, the electron wave function do not collapse and still behave as a wave at the interface (Figure S5b). Its fundamental reason is as follow: the Ag LSPR effect has a strong dipole moment and can transfer energy through dipole-dipole interaction. The free-electron oscillations on ZnO surface (although it is an n-type semiconductor) can produce a very weak dipole moment. Therefore, only a small amount of energy can be transferred. Most of the energy is lost in non-radiation form. However, PDA has a large number of free π electrons, which can be induced by Ag to produce much stronger oscillating electric fields that cover the entire surface of the material. Thus, the LSPR electric field of Ag can no longer be approximated in quasi-particle, that is, the original localized electron wave function behaves as a divergent wave. The electron wave functions of Ag and ZnO are continuous at the interface, which is advantageous to direct charge excitation. The strength of the dipole-dipole interaction can be obtained from equation (S1).[10]

$$E(\text{dipole}-\text{dipole}) \propto \frac{\mu_D \cdot \mu_A}{R_{DA}^3} \qquad (S1)$$

where E is the strength of the dipole-dipole interaction, μ_D and μ_A are the transition dipole moment of donor and acceptor respectively, R^3_{DA} is the distance between donor and acceptor. Because of the difference in surface charge density, $\mu_{Ag} > \mu_{PDA} >> \mu_{ZnO}$.

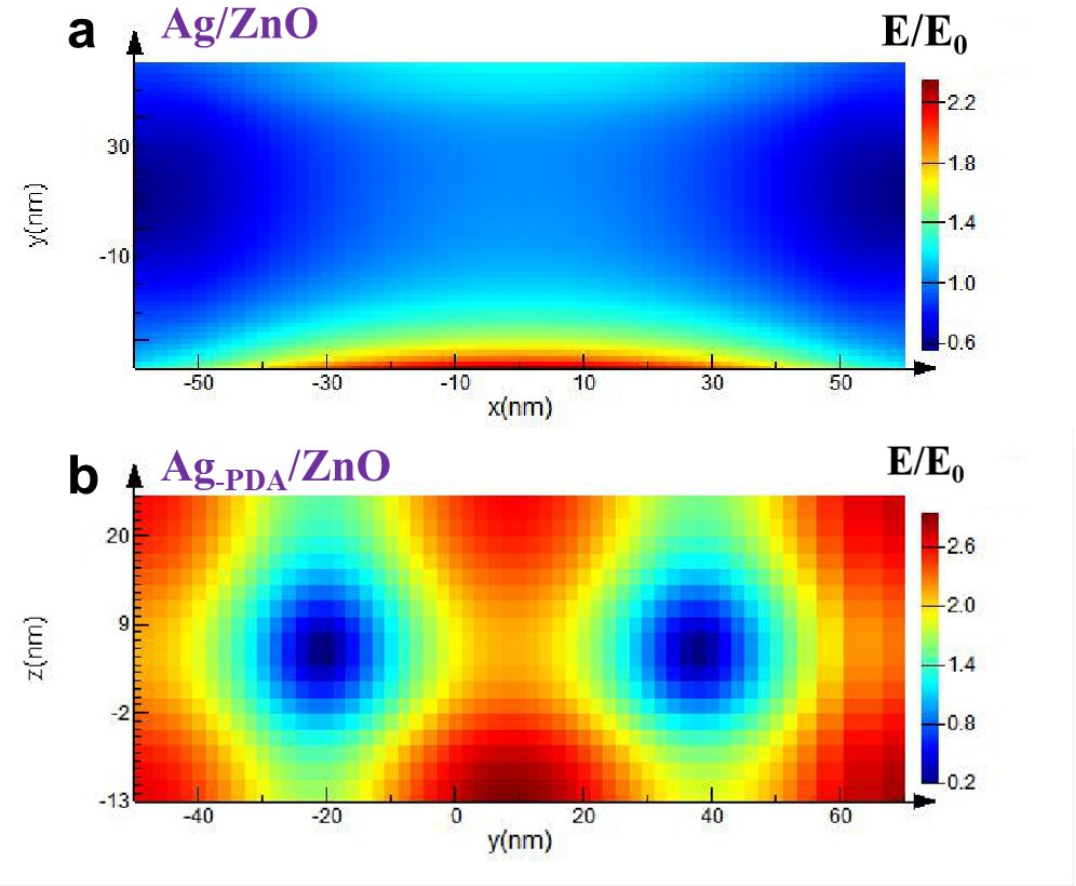

Figure S5: FDTD surface electric field simulation results, a, Ag/ZnO, **b,** $Ag_{\text{-PDA}}$/ZnO. The simulations were performed in a three-dimensional grid measuring 120×120×60 nm. Periodic boundary conditions (PBC) were used for the x- and y-axis directions and a perfectly matched layer (PML) was used in the z-axis direction. A TM polarized plane light was incident on the surface at a 90° angle, with a wavelength range of 400-900 nm. The space between the grid points was 2 nm. The Ag particles were spherical with a diameter of 10 nm. The spacing of the

Ag was large enough so that the coupling effect on the near-field distribution could be ignored. The thickness of the PDA was 5 nm. PDA and Ag were added to the ZnO surface in turn. The dielectric function for Ag and PDA was obtained from data published by Rakic et al.[11] and Khlebtsov et al.[12] The light source was simulated sunlight and illuminated the surface of ZnO vertically.

We further illustrated the direct electron transfer mechanism (Figure S6). The electrons in Ag, extended π bond of PDA, and surface states of ZnO oscillate in the photoelectric field. The degree of light-induced electron clouds overlap will change with a certain frequency. When there is high overlap, the wave functions which were initially highly localized would be connected at the interface, so the electron transfer would be also accompanied by a change in the nucleus and electron configuration. According to the Maxwell equations, this time-varying photoelectric-field-related electron transfer is a wave process. The amplitude of the Ag LSPR effect is much larger than that of ZnO, so the direct electron excitation transfer from Ag to ZnO. On the contrast, the electron clouds overlap generated by conventional indirect transfer mechanism depends on the electronic orbital vibration, which relies on atomic nucleus thermal vibration. This random thermal-related electron transfer can not generate plasmonic waves. In particular, the energy transfer efficiency of LSPR can be evaluated by Fermi's Golden Rule (equation S2).[13] The electron transfer between Ag and ZnO is strictly prohibited under the zero-order approximation. The first-order approximation correction is accomplished by adding the interface electric field coupling term to the H_e operator. The value of the

matrix $\langle \Psi_{Ag*}\Psi_{ZnO}|H_e|\Psi'_{Ag}\Psi'_{ZnO*}\rangle$ depends on the electric field strength. In Figure S5b, PDA provides such a strong electric field coverage. Since the electric field is a vector, it has no contribution to the inverse operation of the matrix. In contrast, the indirect transfer mechanism via adding electronic orbital vibration coupling term to H_e operator caused by thermalization is non-directional, so a large number of reverse transfer of electrons will also accompany in the process. Moreover, the matrix $\langle \Psi_{Ag*}\Psi_{PDA}|H_d|\Psi_{Ag}\Psi_{PDA*}\rangle$ also has a high value because the PDA has many free π electrons that overlap well with the Ag to produce a spatial dipole electric field. LSPR can directly induce the electrons in PDA to excite to a high potential energy surface. For the stable PDA, these excited electrons will eventually return to the high vibration levels of the ground state.[14] At this time, a large number of hot electrons in PDA would show plasmon characteristics, but their disordered band structure greatly delays the thermalization process. Based on the above research, it can be concluded that PDA plays two important roles in the system. One is to inhibit the reverse transfer process so that electrons and holes can accumulate continuously. The other is to transfer originally highly localized quasi-particle-electromagnetic-field to plasmonic wave, thus promoting the direct electron excitation.

$$k_{et} \propto \alpha\left\langle \Psi_{Ag*}\Psi_{ZnO}\left|H_e\right|\Psi'_{Ag}\,\Psi'_{ZnO*}\right\rangle^2 + \beta\left\langle \Psi_{Ag*}\Psi_{PDA}\left|H_d\right|\Psi_{Ag}\Psi_{PDA*}\right\rangle^2 \qquad \text{(S2)}$$

where H_e is the electron transfer operator, which is proportional to *exp(-R)*. R is the distance between the Ag and ZnO; H_d is the dipole-dipole energy transfer operator, which can be calculated by the Förster theory;[10] the operator is proportional to the product of the dipole moment in the optical field $\mu_{Ag}\cdot\mu_{PDA}$.

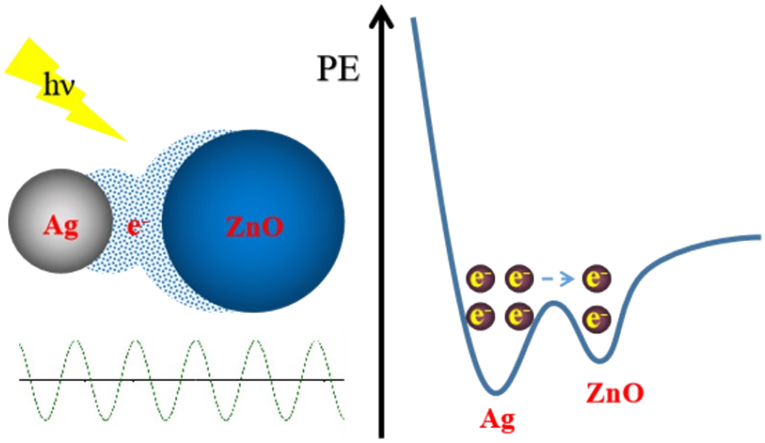

Figure S6: Schematic diagram of time-varying electric-field-related direct electron transfer.

XPS and UPS Spectra

Figure S7a-i shows the XPS and UPS results. The results of the Ag 3d and O 1s spectra are unreliable with regard to the charge transfer mode because the binding energies of Ag 3d are determined by the screening of the core hole, and the O 1s spectra are affected by surface hydroxyl oxygen. The Zn 2p orbital is not screened. A comparison of the XPS results (Figure S7f-h) shows that the negative chemical shift of Ag_{-PDA}/ZnO with respect to pure ZnO is about 10 times that of Ag/ZnO. Furthermore, the UPS results (Figure S7i) show that the surface PDA layer reduces the surface work function of the material by about 0.32 eV. These experimental results indicate that PDA significantly tunes the surface electronic structure.

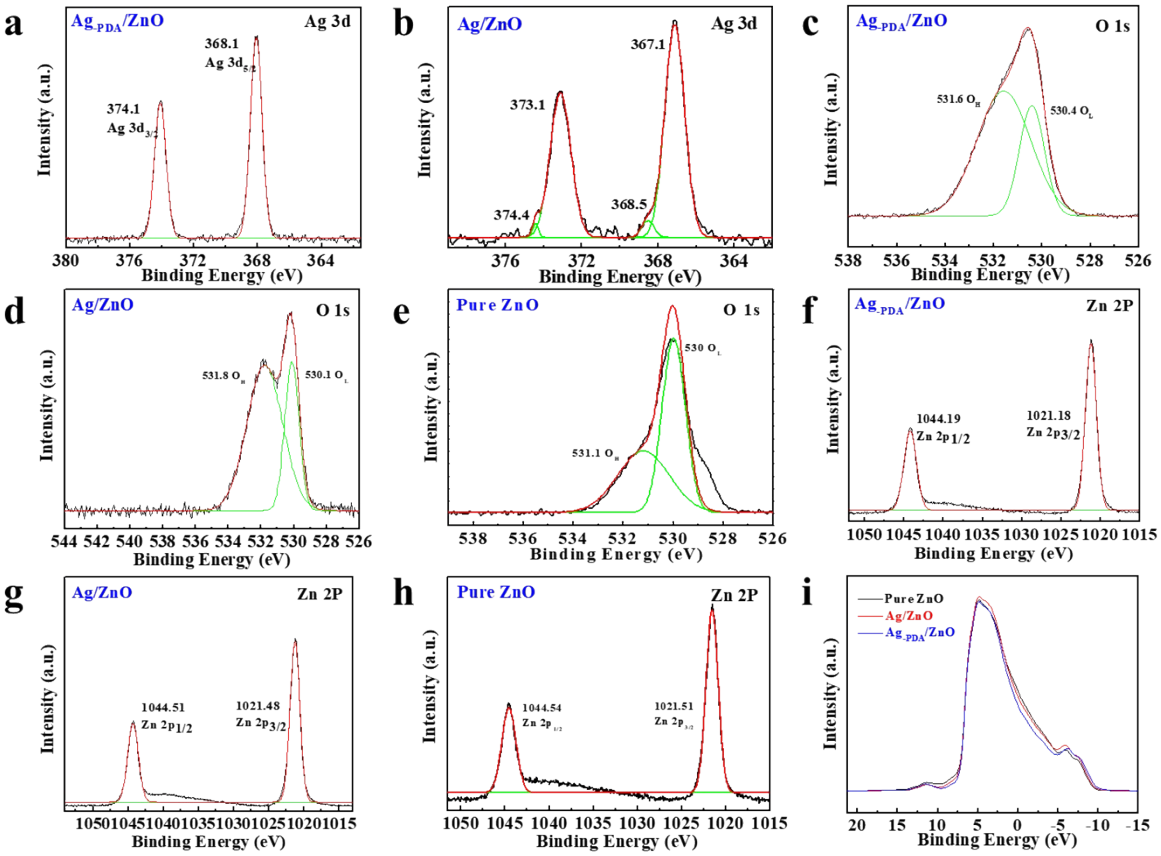

Figure S7: XPS spectra. **a,b,** Ag 3d of Ag/ZnO and Ag_{-PDA}/ZnO. **c-e,** O 1s of pure ZnO, Ag/ZnO and Ag_{-PDA}/ZnO. **f-h,** Zn 2p spectra of pure ZnO, Ag/ZnO, and Ag_{-PDA}/ZnO; The

fitting results of characteristic peak binding energy is labeled in the figure. **i,** UPS spectra of pure ZnO, Ag/ZnO, and Ag_{-PDA}/ZnO; the calculated results of the surface work function are 5.06, 5.04, and 4.74 eV, respectively.

SPV and SPP Spectra

In the SPV results (Figure S8a), the positive voltage decreases, indicating that the electron concentration on ZnO surface increases, which is consistent with the EPR results. In the phase angle spectrum (Figure S8b), unlike the pure ZnO and Ag/ZnO, the Ag_{-PDA}/ZnO shows fluctuations in the visible region. The frequent change in the phase difference indicates that the diffusion distance and the lifetime of the holes vary greatly, which proves that PDA inhibits the thermal relaxation process and stores holes in a series of HOMO-LUMO structures. This result is in agreement with the results of EPR regarding electron storage.

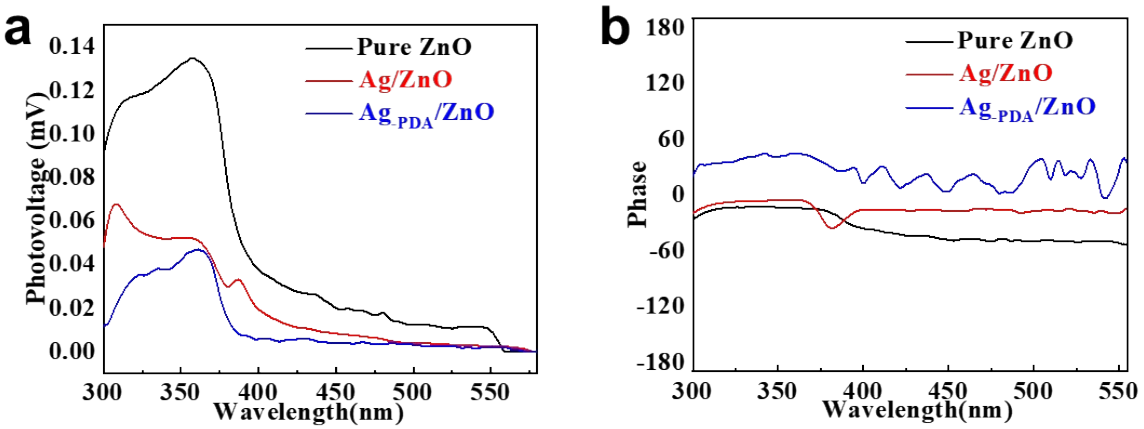

Figure S8: a, SPV of pure ZnO, Ag/ZnO, and Ag_{-PDA}/ZnO; the photovoltage of the pure ZnO is positive, whereas that of Ag_{-PDA}/ZnO is the weakest. **b,** SPP of pure ZnO, Ag/ZnO, and Ag_{-PDA}/ZnO. The test system includes: light source (500W xenon lamp), grating spectrochromator (SPB 500), phase-locked amplifier (SR830-DSP), chopper (SR540). The frequency is 23 Hz, and the scanning speed is 30 nm/min. The system phase Angle error was corrected using an UV-enhanced silicon detector (DSi200) with a 30 μs response time.

EPR and Raman results of Ag/PDA, PDA/ZnO and pure ZnO

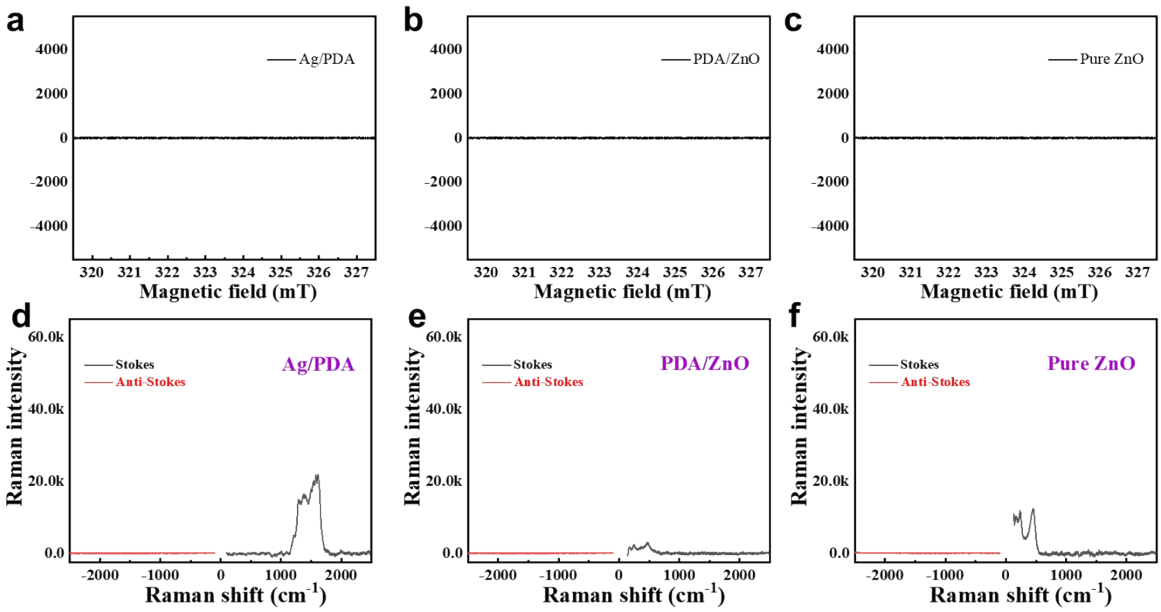

Figure S9: a-c, The EPR results of Ag/PDA, PDA/ZnO and pure ZnO under 532 nm irradiation after 10 min. In the absence of spin traps, the unpaired electrons in Ag/PDA, PDA/ZnO and pure ZnO are too short-lived to be detected, and thus unable to enter the Marcus inverted region. **d-f,** The Raman results of Ag/PDA, PDA/ZnO and pure ZnO excited by 532 nm laser. PDA can tune the Ag electronic structure and produce a variety of vibration modes, showing a wide range of Raman effect. The failure of all thermal phonon modes to generate anti-Stokes signals suggests that direct electronic excitation between Ag and ZnO is necessary.

Details of H_2 and O_2 Yield Under Different Wavelengths and Power

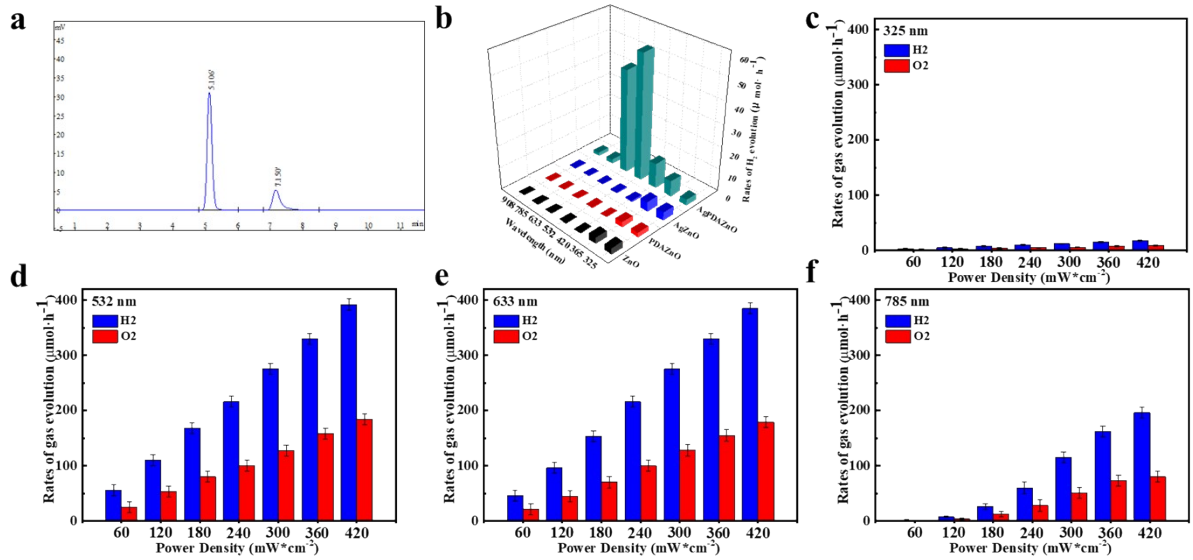

Figure S10: a, The original GC spectrum for one of the tests. The system keep operating, with a cycle every 10 min. The first 4 min ensures that there is no leakage and no impurity gas in the device. The actual retention time of H_2 and O_2 in the column was about 66 s and 188 s, respectively. **b,** H_2 yield of ZnO, PDA/ZnO, Ag/ZnO and Ag_{-PDA}/ZnO under each wavelength irradiation. **c-f,** The incident power-dependent H_2, O_2 yield under each wavelength irradiation. For each set of parameters, the system runs for 1 hour, after which data collection begins. **c,** 325 nm. **d,** 532 nm. **e,** 633 nm. **f,** 785 nm. The result is the average of 20 tests, and the yield of H_2 is twice that of O_2.

Table S2 The incident power-dependent H_2/O_2 yield ($\mu mol \cdot h^{-1}$) under each wavelength irradiation. The result is the average of 20 tests.

Wavelength (nm) /power (mW)	325	532	633	785
60	2.54/1.31	55.8/25.6	46.1/21.3	1.72/0.75

120	4.81/2.53	109.7/53.1	96.3/45.0	7.21/3.53
180	7.52/3.69	168.3/80.8	153.1/70.8	26.5/12.4
240	9.9/4.7	216.9/100.6	216.2/100.7	60.8/28.4
300	11.8/5.7	274.8/126.6	275.0/128.1	115.1/51.3
360	15.3/7.6	330.4/158.7	330.4/155.2	162.4/73.7
420	17.5/8.8	391.6/184.2	385.8/179.3	196.4/80.2

Table S3 The H_2/O_2 yield (μmol•h^{-1}) of ZnO, PDA/ZnO, Ag/ZnO and Ag_{-PDA}/ZnO under each wavelength irradiation. The result is the average of 20 tests.

Wavelength (nm) /Sample	325	365	420	532	633	785	908
ZnO	2.77/1.40	2.76/1.41	0/0	0/0	0/0	0/0	0/0
PDA/ZnO	1.91/0.81	2.05/0.93	0/0	0/0	0/0	0/0	0/0
Ag/ZnO	3.63/1.80	4.14/2.02	0.42/0.20	0.11/0.05	0/0	0/0	0/0
Ag_{-PDA}/ZnO	2.54/1.31	7.05/3.35	11.5/5.24	55.8/25.6	46.1/21.3	1.72/0.75	1.41/0.68

Photoelectrochemical Measurements

The photoelectrochemical performance was measured on a electrochemical workstation. A three-electrode system was employed to analyze the photoelectric current. The sample was coated on conductive glass as a working electrode. A Pt electrode was used as the counter electrode and the saturated calomel electrode (SCE) electrode as the reference electrode. The custom xenon lamp light was employed as the light source (excitation wavelength: 325, 365, 420, 532, 633, 785, 908 nm, output power: 600 W•m^{-2}). The electrolyte used in all measurements was an aqueous solution containing 0.2 mol•L^{-1} Na_2SO_4 at a pH value of 6.8.

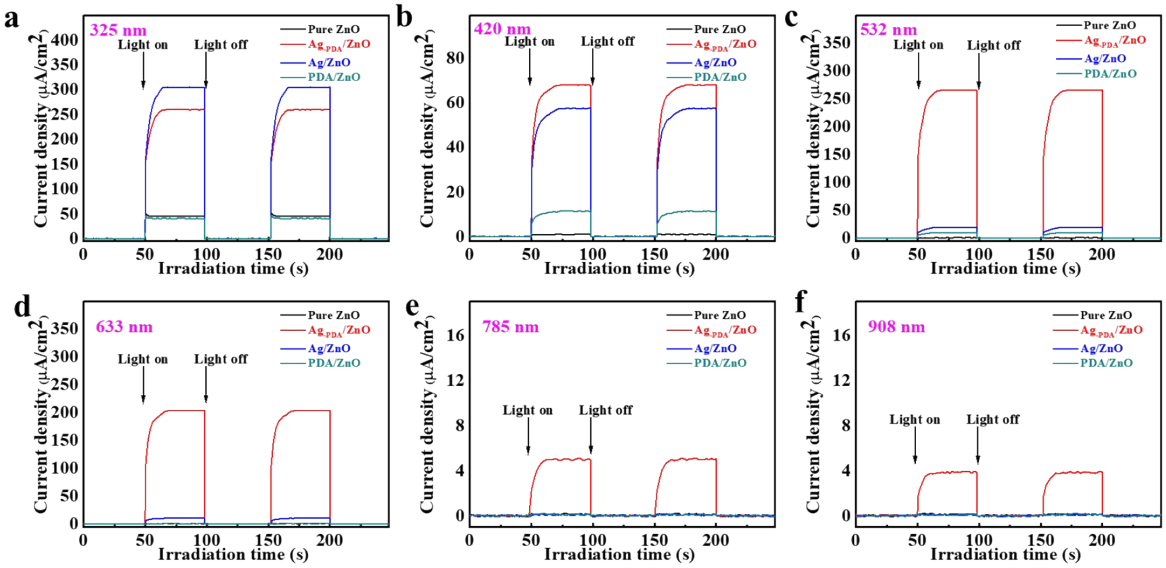

Figure S11: Transient photocurrent results of pure ZnO, Ag/ZnO, PDA/ZnO and Ag$_{PDA}$/ZnO at different wavelength. a, 325 nm. **b,** 420 nm. **c,** 532 nm. **d,** 633 nm. **e,** 785 nm. **f,** 908 nm.

Synergy within the Ternary System

The direct electron excitation is the key for upconversion. The electron transition moment is related to the overlap of initial and final wave function $\langle \Psi_i | \Psi_f \rangle$. Since Ψ_f corresponds to the electron transfer from metal to semiconductor, Ψ_i has the same direction and is conducive to the transition process, which is usually determined by the surface work function of the material. Therefore, the system needs a metal with lower surface work function than a semiconductor. (Pt and TiO_2, the most commonly used materials, are clearly inappropriate). In addition, the semiconductor also needs to be stable and requires a high band gap width to avoid electron-hole pair recombination. Considering the practical significance, the best choices at present to meet these conditions are Ag and ZnO. Furthermore, the use of PDA is creative. PDA is one of the main components of melanin, and its primary advantage is that its inherent structural disorder can greatly extend the lifetime of hot electrons and hot holes and prevent their radiation deactivation process.[15] We suspect that the lifetime could even be days, but this has not been proven due to technical limitations. Another advantage of PDA is that dopamine molecules can coordinate with Ag^+ and Zn^{2+} to form strong interaction in its self-aggregation process. And the polymerization process of dopamine can be also easily regulated by controlling the temperature and oxygen content in the solution to form a suitable ternary system with Ag and ZnO during in-situ photoreduction process.

More importantly, Ag is easily oxidized during the catalysis process and its stability is insufficient. However, the fastest time for Ag to react with surface-adsorbed molecules (H_2O, O_2, etc,.) is on the order of picoseconds, whereas the direct transfer process occurs in femtoseconds or even less. Therefore, when electrons and holes have long enough lifetimes,

the final reaction between the carrier and the molecule can be achieved by a multi-electron transfer process,[16] which avoids the formation of free radicals. Combined with the XRD and XPS results (Figure S12a,b, and Figure 5d,e), the OER should be included two pathways (equation S3, S4).

$$\begin{aligned} &h^+ + H_2O \rightarrow \bullet OH + H^+ \\ &Ag + \bullet OH \rightarrow Ag_2O \\ &2Ag_2O \rightarrow 2Ag + O_2 \\ &2H^+ + 2e^- \rightarrow H_2 \end{aligned} \tag{S3}$$

$$\begin{aligned} &4h^+ + 2H_2O \xrightarrow{Ag} 4H^+ + O_2 \\ &4H^+ + 4e^- \rightarrow 2H_2 \end{aligned} \tag{S4}$$

Firstly, Ag surface would inevitably be oxidized, while Ag_2O easily decomposes into Ag and O_2 under light irradiation, and their balance depends on the surface oxygen partial pressure. Equation S3 represents a general reaction pathway. However, when the reaction enter the Marcus inverted region, a plenty number of photogenerated-holes would cause Ag_2O unable to exist stably, so reaction can transfer four electrons in one step on Ag surface, and its process would not form hydroxyl radicals and Ag_2O intermediates (i.e., equation S4). In Ag/ZnO, the diffraction peaks of Ag_2O in XRD results (Figure S12a) and the change of Ag chemical state in XPS spectra (Figure 5d) supports the equation S3 pathway. While in Ag_{-PDA}/ZnO (Figure S12b, and Figure 5e), its stable chemical state supports OER are mainly four-electrons-transferring process. Since the formation of free radicals requires extra energy input, and they also destroy the structure of materials, this four-electrons-transferring in one step reaction mechanism is stable and efficient by comparison. Note that the holes concentration is

insufficient to completely inhibit Ag_2O formation under ordinary light source. A higher holes concentration requires to increase the incident power. When Ag_2O no longer exists, free holes on Ag surface reach the saturation limit, corresponding to the OER extreme efficiency, which is consistent with the results in Figure 5 b,c. In short, HER and OER occur on Ag and ZnO surfaces, respectively. In the presence of PDA passivation layer, femtosecond excited electron-hole can not reverse transfer (equation S2), so the synergistic effect of ternary system is essential.

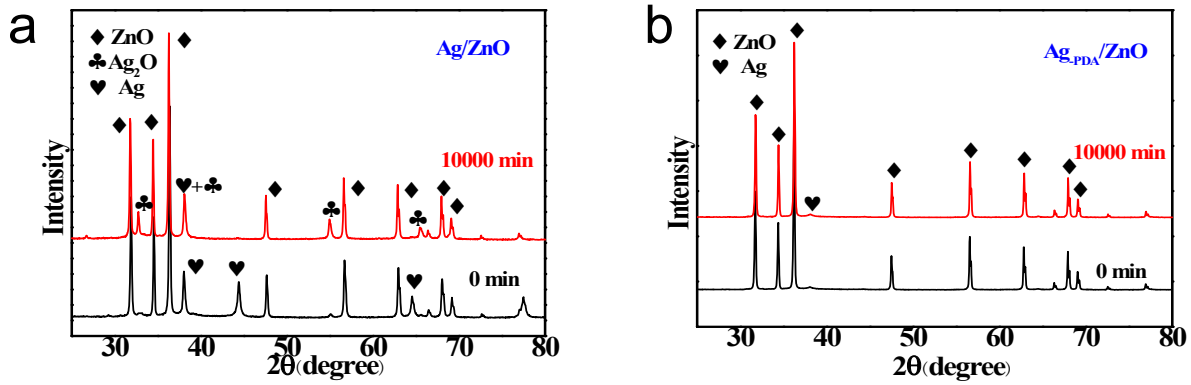

Figure S12: a,b, XRD results of Ag/ZnO and Ag_{-PDA}/ZnO before and after working 10000 min under AM 1.5G. In Ag/ZnO, Ag is oxidized to Ag_2O in overall water splitting. In Ag_{-PDA}/ZnO, although the amorphous structure of PDA makes the peak with weak strength even less obvious, it can still be seen that Ag hardly changes after 10000min operation.

The Action Time of Photons at Different Wavelengths

The time interval between the ground state and the excited state of the electron promoted by light is estimated by the Heisenberg uncertainty principle (derivation process see equation S5-S7).

$$\delta t \times \delta E \geq h/4\pi \quad (S5)$$

$$E = hc/\lambda \quad (S6)$$

$$\delta t \geq \lambda/4\pi c \quad (S7)$$

Table S4 The action time of photons at different wavelengths

Wavelength (nm)	325	365	420	532	785
Action time (s)	0.862×10^{-16}	0.968×10^{-16}	1.114×10^{-16}	1.411×10^{-16}	2.082×10^{-16}

References

1. L. Zhou, D. F. Swearer, C. Zhang, H. Robatjazi, H. Zhao, L. Henderson, L. Dong, P. Christopher, E. A. Carter and P. Nordlander, *Science*, 2018, **362**, 69-72.
2. X. Zhang, M. Wang, F. Tang, H. Zhang, Y. Fu, D. Liu and X. Song, *Advanced Science*, 2020, **7**, 1902408.
3. Z. Zhang, C. Zhang, H. Zheng and H. Xu, *Accounts of Chemical Research*, 2019, **52**, 2506-2515.
4. R. Zhang, L. Bursi, J. D. Cox, Y. Cui, C. M. Krauter, A. Alabastri, A. Manjavacas, A. Calzolari, S. Corni and E. Molinari, *ACS Nano*, 2017, **11**, 7321-7335.
5. A. Campos, N. Troc, E. Cottancin, M. Pellarin, H.-C. Weissker, J. Lermé, M. Kociak and M. Hillenkamp, *Nature Physics*, 2018, **15**, 275-280.
6. K. Wu, J. Chen, J. R. McBride and T. Lian, *Science*, 2015, **349**, 632-635.
7. J. Wang, T. Ding, Kaimin Gao, L. Wang, P. Zhou and K. Wu, *Nature Communications,* 2021, **12**, 6333.
8. E. Kazuma and Y. Kim, *Angewandte Chemie*, 2019, **58**, 4800-4808.

9. Y. Zhang, S. He, W. Guo, Y. Hu, J. Huang, J. R. Mulcahy and W. D. Wei, *Chemical Reviews*, 2017, **118**, 2927-2954.

10. G. Scheibe, *Angewandte Chemie*, 1954, **66**, 164-164.

11. A. D. Rakic, A. B. Djurisic, J. Elazar and M. L. Majewski, *Applied Optics*, 1998, **37**, 5271-5283.

12. B. N. Khlebtsov, A. M. Burov and N. G. Khlebtsov, *Applied Materials Today*, 2019, **15**, 67-76.

13. A. Manjavacas, J. G. Liu, V. Kulkarni and P. Nordlander, *ACS Nano*, 2014, **8**, 7630-7638.

14. A. Umar, V. G. Rao, C Steven and L. Suljo, *Nature Catalysis*, 2018, **1**, 656-665.

15. J. Li and K. Pu, *Chemical Society Reviews*, 2019, **48**, 38-71.

16. M. A. Bowring, L. R. Bradshaw, G. A. Parada, T. P. Pollock, R. Fernandezteran, S. S. Kolmar, B. Q. Mercado, C. W. Schlenker, D. R. Gamelin and J. M. Mayer, *Journal of the American Chemical Society*, 2018, **140**, 7449-7452.